RSC Advances

PAPER

View Article Online
View Journal | View Issue

Cite this: *RSC Adv.*, 2015, **5**, 50253

Non-covalent functionalization of carbon nano-onions with pyrene–BODIPY dyads for biological imaging†

Juergen Bartelmess,‡[a] Marco Frasconi,‡[a] Preethi B. Balakrishnan,[b] Angelo Signorelli,[a] Luis Echegoyen,[c] Teresa Pellegrino[b] and Silvia Giordani*[a]

Received 27th April 2015
Accepted 29th May 2015

DOI: 10.1039/c5ra07683h

www.rsc.org/advances

We report a novel approach based on non-covalent interactions for the functionalization of carbon nano-onions (CNOs) with fluorophores. The assembly of pyrene–BODIPY conjugates on the CNO surface by means of π–π-stacking results in fluorescent carbon nanoparticles that are successfully uptaken by HeLa cancer cells with no cytotoxicity observed. The ability to functionalize carbon-based nanomaterials by using mild conditions will pave the way for future clinical application of these versatile nanomaterials.

1. Introduction

Nanoprobes as imaging agents are of great interest in biomedicine and for the study of biological systems.[1,2] In this regard, carbon nanomaterials have attracted considerable attention over the last few years.[3–6] Multi-shell fullerenes, also known as carbon nano-onions (CNOs),[7] are promising materials for biomedical imaging investigations. Recently, we have reported[8–10] a series of CNOs covalently functionalized with different fluorophores which were bound to benzoic acid groups[11] on the CNO surface by amidation or esterification reactions. In-depth toxicological studies performed *in vitro* as well as *in vivo* with fluorescein–CNO conjugates, revealed low cytotoxicity and low inflammatory response.[8] The good biocompatibility and the low cytotoxicity render these nanomaterials as promising candidates for future applications in biology and medicine. CNOs functionalized by either a covalent approach or with polymeric matrices have been successfully applied also in other fields of scientific research.[12]

In the present study, we investigated for the first time the non-covalent functionalization of pristine CNOs (**p-CNOs**) with small molecules such as pyrene derivatives. The use of π–π-interactions for the non-covalent functionalization of carbon nanotubes (CNTs) with molecules bearing extended π-systems is a well-established protocol.[13] Prominent examples include the immobilization of metal complexes,[14,15] crown ethers,[16,17] tetrapyrrole macrocycles,[18–22] and guanosine derivatives.[23] Also the immobilization of pyrene derivatives on the sidewalls of CNTs promoted by π–π-stacking has been extensively studied.[24] Pyrene is well-suited for this purpose and catalytically active metal complexes are important examples.[25–27] In addition, several pyrene–chromophore/CNT hybrids were reported, with prominent examples including pyrene–phthalocyanine[28] and pyrene–porphyrin[29,30] derivatives. One example of a boron dipyrromethene (BODIPY)–pyrene/CNT hybrid was described by Erbas *et al.*, who immobilized a pyrene-derivatized di-styryl expanded BODIPY derivative on the sidewalls of CNTs.[31] In this report, we exploit pyrene as an anchoring group in a novel pyrene–BODIPY dyad, compound **3** in Scheme 1, for the non-covalent functionalization of **p-CNOs**. BODIPY dyes are well known for high fluorescence quantum yields, synthetic versatility and high photostability.[32–34] The modification of **p-CNOs** with **3** yields a fluorescent hybrid system, **p-CNO/3**, which is held together by π–π-interactions between the pyrene unit of **3** and the extended aromatic system on the surface of the **p-CNOs** (Scheme 1). While the primary focus of this study was cellular imaging and the elucidation of the cell internalization pathways of the fluorescent CNO constructs, the long term perspective is to use them for drug delivery, in combination with cellular imaging.

2. Experimental

All reagents used for the synthesis were purchased from Sigma-Aldrich and used as received. All solvents were purchased from Sigma-Aldrich and of ACS or HPLC grade and used as received, unless otherwise noted. DMF was dried over activated 4 Å molecular sieves (Sigma-Aldrich). All reactions and

[a]*Istituto Italiano di Tecnologia (IIT), Nano Carbon Materials Lab, Via Morego 30, 16163 Genova, Italy. E-mail: silvia.giordani@iit.it*

[b]*Istituto Italiano di Tecnologia (IIT), Drug Discovery and Development Department, Via Morego 30, 16163 Genova, Italy*

[c]*University of Texas at El Paso, Department of Chemistry, 500 W. University Ave., El Paso, TX 79968, USA*

† Electronic supplementary information (ESI) available: Additional technical and biological procedures, utilized materials and instrumentation, additional FT-IR, absorption and fluorescence spectra and spectroscopic data. Additional confocal microscopy images. See DOI: 10.1039/c5ra07683h

‡ These authors contributed equally to this work.

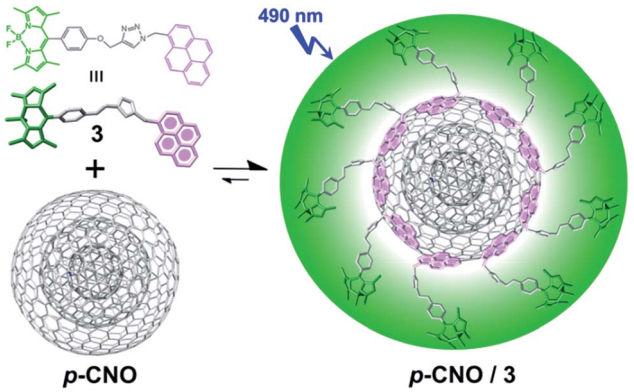

Scheme 1 Non-covalent assembly of p-CNO/3.

measurements were carried out under ambient conditions, unless otherwise noted.

Synthesis

3. **1** (ref. 35) (75.6 mg, 0.20 mmol), **2** (ref. 36) (54.5 mg, 0.21 mmol) and sodium ascorbate (23.8 mg, 0.12 mmol) were dissolved in 20 mL dry DMF and purged with nitrogen. Copper(I) iodide (11.4 mg, 0.06 mmol) was added and the reaction was stirred at 60 °C for 16 h in the dark under a N_2 atmosphere. After cooling to room temperature, the reaction mixture was poured into 50 mL brine and extracted with 3 × 30 mL dichloromethane. The combined organic phases were washed with water (2 × 50 mL) and brine (1 × 50 mL) and dried over $MgSO_4$. The solvent was evaporated and the crude was purified by column chromatography (SiO_2, eluted with hexane: dichloromethane (1 : 3, v/v), then dichloromethane and finally dichloromethane containing 5% ethyl acetate). **3** was obtained as an orange solid (102.5 mg, 0.16 mmol, 80%). ^{1}H NMR (400 MHz, $CDCl_3$) δ 8.60–8.00 (m, 9H, *pyrene-H*), 7.39 (s, 1H, *triazole-H*), 7.07 (m, 2H, *Ar–H*), 6.97 (m, 2H, *Ar–H*), 6.29 (s, 2H, $-CH_2$), 5.90 (s, 2H, *pyrrole-H*), 5.13 (s, 2H, $-CH_2$), 2.53 (s, 6H, $-CH_3$), 1.28 (s, 6H, $-CH_3$). ^{13}C NMR (100 MHz, $CDCl_3$) (14.4, 14.6, 52.7, 62.1, 115.4, 116.7, 121.1, 121.9, 122.7, 125.0, 125.9, 126.1, 126.4, 126.5, 127.2, 127.8, 128.5, 129.2–129.4 (multiple peaks), 130.6, 131.2, 132.3, 141.5, 143.1, 155.3, 158.2, 158.7). UV-Vis (toluene) λ_{max} (ε [$\times 10^3$ M^{-1} cm^{-1}]) 316 (14.8), 330 (32.3), 346 (46.6), 503 (94.7) nm. UV-Vis (DMSO) λ_{max} (ε [$\times 10^3$ M^{-1} cm^{-1}]) 268 (30.3), 279 (47.2), 316 (14.8), 330 (32.4), 346 (47.4), 501 (87.0) nm. HRMS-ESI: *m*/*z*: calcd for $C_{39}H_{33}BF_2N_5O^+$: 636.2746 $[M + H]^+$, found: 636.2762.

p-CNO. The preparation of pristine CNOs was performed as previously described.[37]

Benz-CNO. The procedure for benzoic acid functionalized CNOs was published earlier.[10] In the present report the workup procedure was modified. Sodium nitrite (2.45 g, 35.5 mmol) was dissolved in 30 mL of deionized water and combined with 4-aminobenzoic acid (4.80 g, 35 mmol) in 40 mL of DMF at 0 °C. 0.5 mL of concentrated HCl were added and the reaction mixture was stirred for 30 min at 0 °C. Then pristine CNOs (52 mg), dispersed in 50 mL DMF by sonicating for 20 minutes, were added and stirred for 4 h at 0 °C and additional 3 days at room temperature. Following this, the CNOs were recovered by filtration with a 0.2 μm nylon membrane and extensive washing with water, DMF, methanol, acetone and tetrahydrofuran. After drying at room temperature for several days, 51 mg of **benz-CNO** were recovered.

p-CNO/3. 3 (4 mg, ~0.006 mmol) and 12 mg of **p-CNO** were dispersed in 20 mL of dry DMF and sonicated in an ultrasonic bath for 60 minutes. Then, the CNOs were filtered through a polyamide filter (0.2 μm) and extensively washed with THF until the THF appears colorless (approx. 100 mL). Finally the functionalized CNO nanomaterial was dried overnight at room temperature. 11 mg of **p-CNO/3** hybrid were recovered from the filter as a black, fine powder.

Benz-CNO/3. 3 (4 mg, ~0.006 mmol) and 12 mg of **benz-CNO** were dispersed in 20 mL of dry DMF and sonicated in an ultrasonic bath for 60 minutes. Then, the CNOs were filtered through a polyamide filter (0.2 μm) and extensively washed with THF until the THF appears colorless (approx. 100 mL). Finally the functionalized CNO nanomaterial was dried overnight at room temperature. 11 mg of **benz-CNO/3** hybrid were recovered from the filter as a black, fine powder.

Cytotoxicity assay

Cells were grown in monolayer culture at 37 °C under a 5% CO_2 atmosphere in a humidified environment. HeLa cells were cultured in Dulbecco's modified Eagle's medium (DMEM) enriched with 10% FBS (Life Technologies), 2% Penstrep and 1% glutamine. Cells were seeded in 24 well chamber slides at a density of 5 × 10^4 cells per well and incubated in a 500 μL cell culture medium to obtain a subconfluent monolayer after 48 h in a humidified atmosphere at 37 °C and 5% CO_2. The CNO samples were prepared by suspending 1 mg of sample in 1 mL sterile phosphate buffered saline (PBS) solution followed by sonication for 20 min at 68 kHz (50%). The samples were then dispersed in the cell culture media (DMEM) to attain CNO suspensions at final concentrations of 2, 5, 10, 20 μg mL^{-1}. The viability test of the HeLa cells exposed for different times to the samples of CNOs was evaluated *versus* a control experiment, utilizing the PrestoBlueTM cell viability assay (Life Technologies). Assays were performed following a procedure reported previously,[38] based on the measurement of the absorbance at 570 nm on a microplate reader. Each measurement was normalized with the average signal of control experiment (untreated cells) and the percent of cell viability was expressed as the mean ± SD.

Cellular imaging

Confocal imaging was performed with a laser scanning confocal microscope equipped with a resonant scanner (Nikon A1R). HeLa cells were treated with different concentration of CNO samples and followed by staining with LysoTracker Red DND-99, a dye that tags endosomes and lysosomes, and Hoechst 33342, for live nuclear staining. The samples were then fixed with 4% paraformaldehyde. Excitation of the BODIPY on the CNO samples was performed at 488 nm and the emission was

acquired in the spectral window between 500–560 nm. The Lysotracker Deep Red was exited at 577 nm, while the Hoechst 33342 was exited at 405 nm and the images were acquired, respectively, in the emission range of 600–680 nm and 415–480 nm.

3. Results and discussion

The pyrene–BODIPY dyad **3** was synthesized by a copper mediated *Huisgen* type "click"-reaction between propargyl functionalized BODIPY derivative **1** (ref. 35) and 1-(azidomethyl) pyrene **2** (ref. 36) in 80% yield (Scheme 2).

The successful preparation of **3** was confirmed by UV-Vis absorption, fluorescence, FT-IR, ^{1}H and ^{13}C NMR spectroscopy as well as by high resolution mass spectrometry. The absorption maximum of **3** in DMSO is located at 501 nm with an emission maximum at 513 nm and a high fluorescence quantum yield of about 0.7. Pyrene-centered absorption features are located in the UV region as illustrated in Fig. 1. Fluorescence spectroscopic studies of **3** evidence an efficient excited state energy transfer from the photoexcited pyrene to the BODIPY moiety, which leads to an almost complete quenching of the pyrene centered fluorescence features (Fig. 1), a phenomenon that was observed previously for a structurally different pyrene–BODIPY dyad and discussed in detail.[39] Comparable photophysical properties were exhibited by anthracene–BODIPY dyads.[40]

BODIPY **3** revealed a significant solvent dependency of the fluorescence lifetime when comparing the data obtained for **3** in DMSO with toluene. While in DMSO τ_F of **3** is about 3.75 ns, it is about 3.35 ns in toluene. Fluorescence lifetime measurements of the BODIPY–acetylene precursor **1** show similar τ_F values and a comparable solvent dependency (3.80 ns in DMSO and 3.23 ns in toluene). A rational explanation for this observation is the distance between the pyrene moiety and the BODIPY core as well as the BODIPY's molecular structure and hence the lack of π–π-conjugation between the two functional subunits.

Non-covalent functionalization of small diameter (~5 nm) pristine carbon nano-onions (**p-CNO**)[37] with **3** was accomplished by sonication of **p-CNO** together with **3** in dry DMF, leading to **p-CNO/3** hybrid materials (Scheme 1). The fluorophore loaded CNOs were separated by filtration and washed carefully with THF to remove non-adsorbed dye. With the aim to develop an efficient platform that can be used to deliver drugs in conjunction with targeting or imaging units, we also

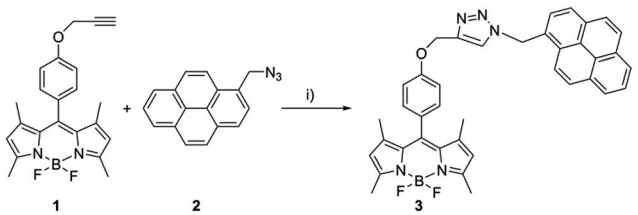

Scheme 2 Synthetic procedure for the synthesis of pyrene–BODIPY dyad **3**. (i) CuI, ascorbic acid, DMF, N_2, 60 °C.

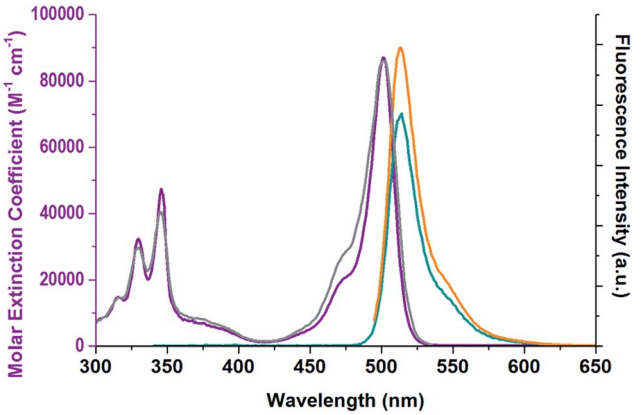

Fig. 1 Absorption (purple) and fluorescence (cyan: excitation of the pyrene moiety at 330 nm; orange: excitation of the BODIPY at 485 nm) spectra of **3** in DMSO. Grey: excitation spectrum of **3** recorded at a fixed emission wavelength of 545 nm, and varied excitation wavelengths to illustrate excited state energy transfer from the photoexcited pyrene to the BODIPY moiety.

evaluated the assembly of compound **3** onto the surface of CNOs, chemically modified with benzoic acid functionalities (**benz-CNO**). Following the functionalization procedure developed for the **p-CNOs**, the supramolecular construct **benz-CNO/3** was prepared.

UV-Vis absorption and fluorescence spectroscopy clearly revealed the presence of CNO immobilized fluorophore **3** (Fig. 2). BODIPY centered absorption and emission, with an absorption maximum at 501 nm and an emission maximum at 511 nm (in DMSO), were observed. A lower coverage of the fluorophore was evidenced for **benz-CNO/3** (blue lines in Fig. 2) in comparison to that for **p-CNO/3** (red lines in Fig. 2) as a consequence of the presence of benzoic acid functionalities on the surface of the **benz-CNO**. Fluorescence lifetime analysis of **p-CNO/3** and **benz-CNO/3**, dispersed in DMSO, revealed values

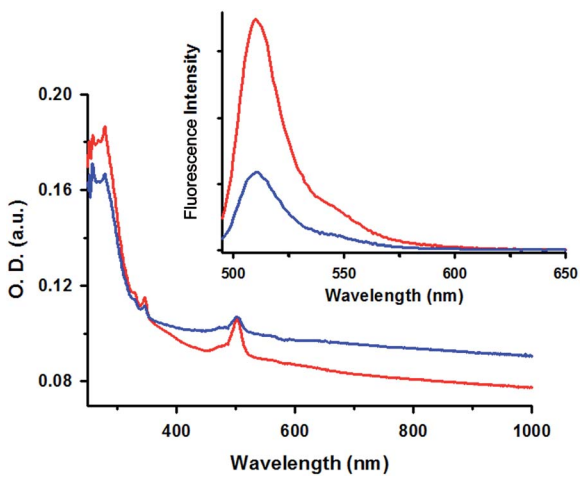

Fig. 2 Absorption spectra of **p-CNO/3** (red line) and **benz-CNO/3** (blue line). Inset: fluorescence spectra of **p-CNO/3** (red line) and **benz-CNO/3** (blue line) excited at 490 nm. Mass concentration: 10 μg mL^{-1}, solvent: DMSO.

of 3.82 ns and 3.68 ns, respectively. The fluorescence quantum yield of a **p-CNO/3** dispersion (10 μg mL^{-1}) was estimated to be about 0.32 (Fig. S1†). The reduction of the fluorescence intensity of **p-CNO/3** compared to that of the free pyrene–BODIPY dyad **3** is well in line with our earlier reported CNO based imaging agents[8–10,41] and is related to the strong plasmonic absorption of the CNO bulk material. The fluorescence intensity is still quite high, especially if compared to other carbon nanomaterial based imaging agents,[3] making the pyrene–BODIPY loaded CNO nanomaterial promising, bright imaging agents for cellular studies. Solid-state ATR FT-IR spectroscopy further corroborated the presence of **3** in the CNO nanomaterials (Fig. S2†). It is important to mention that the non-covalent CNO functionalization with **3** led to a significant increase of the CNO dispersability compared to that of **p-CNO**, presumably due to a reduced tendency to form aggregates. While pristine CNOs cannot be dispersed efficiently in aqueous media at all, aqueous **p-CNO/3** dispersions show sufficient stability to study the cellular uptake.

In order to investigate the potential application of this platform as an imaging probe and for drug delivery applications, we investigated the cellular uptake of the **p-CNO/3** and **benz-CNO/3** nanomaterials *in vitro* using HeLa wild type cervical cancer cells. The cellular viability was tested in the presence of different CNO mass concentrations, ranging from 2 to 20 μg mL^{-1}, by using a resazurin-based assay. The percentage viability is expressed in comparison with a control consisting of cells treated with only the culture media (Fig. 3). **p-CNO/3** showed low cytotoxicity, even up to 72 hours of incubation at 37 °C, and the viability of the HeLa cells was found to be higher than 80% under different conditions (Fig. 3A). A similar trend of the cytotoxicity with the incubation time was observed by treating the HeLa cells with different concentrations of **benz-CNO/3** (Fig. 3B). The low cytotoxicity observed for these fluorescently labelled CNO particles encouraged further cellular imaging studies, with the aim to elucidate the mechanism of uptake and the localization of **p-CNO/3** in the cells. HeLa cells were treated for 30 min at 37 °C with different concentrations of **p-CNO/3**, ranging from 2 to 10 μg mL^{-1}. After this period, the cells were carefully rinsed with fresh media and then fixed with paraformaldehyde. The cells efficiently took up the fluorescently labeled CNOs as demonstrated by confocal microscopy images. At low concentration of **p-CNO/3**, a strong fluorescence signal from the BODIPY was detected in the perinuclear region in a point-like distribution typical of endocytosis uptake (Fig. 4A). A control experiment where the cells were incubated at 4 °C in the presence of **p-CNO/3** was carried out to confirm the uptake mechanism. After 30 min at 4 °C, no significant fluorescence localized in the cells was observed (Fig. 4A, inset), indicating that the internalization of **p-CNO/3** by the cells occurs by an endocytosis pathway and not by passive diffusion through the cell membrane. When HeLa cells were treated at 37 °C with a higher concentration of **p-CNO/3**, 10 μg mL^{-1}, a green fluorescence signal widely spread inside the cells was detected (Fig. 4B). Control experiments, where the cells were incubated at 4 °C show only a minimum uptake of **p-CNO/3** at this higher concentration as confirmed by a slight green fluorescence (Fig. 4B, inset).

The internalization of the **p-CNO/3** by lysosomes was investigated at different concentrations of **p-CNO/3** by staining the lysosomes with the Lysotracker probe. HeLa cells were

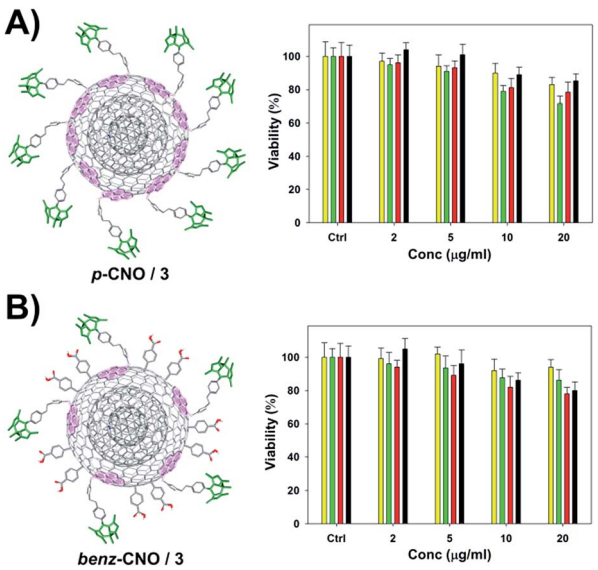

Fig. 3 Cellular viability of HeLa wt cells after exposure to different concentrations (2, 5, 10, 20 μg mL^{-1}) of **p-CNO/3** (A) and **benz-CNO/3** (B). The viability was measured after 12 (yellow), 24 (green), 48 (red) and 72 (black) hours of incubation at 37 °C.

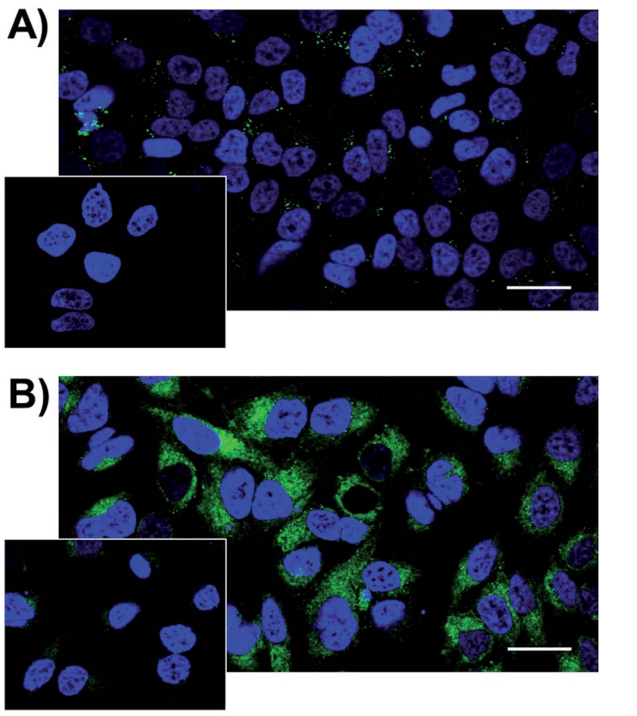

Fig. 4 Confocal images of fixed HeLa cells incubated for 30 min at 37 °C with 2 μg mL^{-1} (A) and 10 μg mL^{-1} (B) of **p-CNO/3**. Cells were stained with Hoechst 33342 (blue). The insets show the corresponding uptake of **p-CNO/3** by HeLa cells incubated at 4 °C.

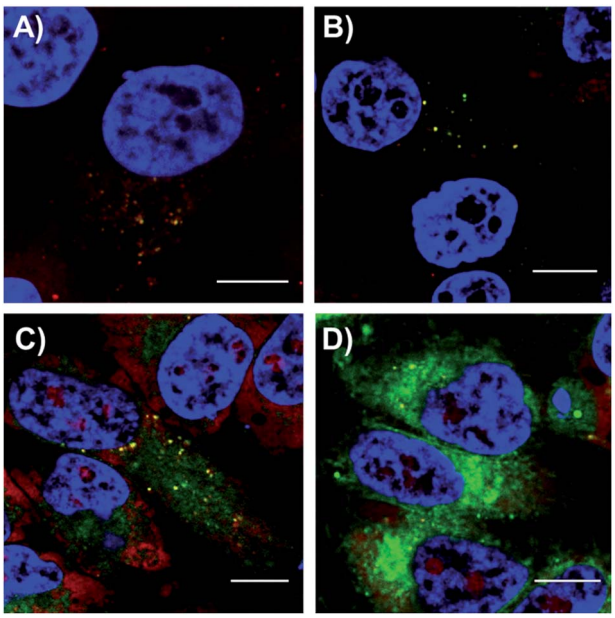

Fig. 5 Confocal images of fixed HeLa cells incubated for 30 min at 37 °C with 2 (A and B), 5 (C) and 10 (D) μg mL^{-1} of **p-CNO/3**. After washing the cells from the excess of **p-CNO/3**, the cells were incubated with fresh media and the confocal was measured immediately (A) or after 2 h of incubation (B)–(D). The nuclei were stained with Hoechst 33342, while lysosomes were stained with Lysotracker red probe. The colocalization of **p-CNO/3** within the lysosomes is indicated in yellow. Scale bar: 10 μm.

incubated for 30 min with **p-CNO/3** at concentration of 2 (Fig. 5A and B), 5 μg mL^{-1} (Fig. 5D) and 10 μg mL^{-1} (Fig. 5D).

Confocal images, taken immediately after washing the cells from the excess of **p-CNO/3**, show yellow colocalization signal confirming that the CNO constructs localize in lysosomal vesicles (Fig. 5A), as previously observed for the CNOs covalently labeled with BODIPY dye.[10] Interestingly, a more diffuse and intense fluorescence signal was observed after incubating the cells in fresh media for an additional 2 hours after treating with **p-CNO/3** at 2 μg mL^{-1} (Fig. 5B). At concentrations of 5 and 10 μg mL^{-1}, green fluorescence was detected also in the cell cytoplasm (Fig. 5C and D). The diffuse fluorescence observed for longer incubation times could be an indication of the slow release of pyrene–BODIPY **3** from the surface of the CNOs upon interaction with the hydrophobic environments within the cell. Investigating the localization of nanomaterials, such as CNOs, and understanding their interactions with specific compartments within the cell is a fundamental aspect for developing efficient probes for cellular imaging.

4. Conclusions

In summary, we demonstrated a versatile approach for the functionalization of the surface of CNOs by using non-covalent π–π-interactions. The novel pyrene–BODIPY **3** was employed to decorate the surface of CNOs, that led to an increase in the CNOs' dispersibility. The successful cellular uptake of the fluorescent **p-CNO/3** and **benz-CNO/3** hybrid material by HeLa cells was confirmed without significant cytotoxic effects. These encouraging results render non-covalently functionalized CNOs as efficient molecular shuttles for future applications for the delivery of hydrophobic drugs as well as for cellular imaging. The combination of multiple functionalization steps will allow for the preparation of tailor made theranostic CNO based nanomaterials, and these studies are currently underway in our laboratories.

Acknowledgements

We are grateful to the Istituto Italiano di Tecnologia (IIT) for funding. We thank Agustin Molina-Ontario (UTEP) for the preparation of the pristine CNOs, Michele Baldrighi (IIT Nano Carbon Materials) for instrumental support, Sine Mandrup Bertozzi (IIT Drug Discovery and Development) for the HR mass spectrometry and Giuseppe Vicidomini (IIT Nanophysics) for the fluorescence lifetime measurements. LE wishes to thank the Robert A. Welch Foundation (Grant AH-0033) and the US National Science Foundation (grant DNR-1205302) for generous financial support.

Notes and references

1 C. M. C. Tempany and B. J. McNeil, *J. Am. Med. Assoc.*, 2001, **285**, 562–567.
2 H. Koo, M. S. Huh, J. H. Ryu, D.-E. Lee, I.-C. Sun, K. Choi, K. Kim and I. C. Kwon, *Nano Today*, 2011, **6**, 204–220.
3 J. Bartelmess, S. J. Quinn and S. Giordani, *Chem. Soc. Rev.*, 2015, DOI: 10.1039/c4cs00306c, Advance Article.
4 F. Baptista, S. A. Belhout, S. Giordani and S. J. Quinn, *Chem. Soc. Rev.*, 2015, DOI: 10.1039/c4cs00379a, Advance Article.
5 Y. Song, S. Zhu and B. Yang, *RSC Adv.*, 2014, **4**, 27184–27200.
6 J. M. Yoo, J. H. Kang and B. H. Hong, *Chem. Soc. Rev.*, 2015, DOI: 10.1039/c5cs00072f, Advance Article.
7 D. Ugarte, *Nature*, 1992, **359**, 707–709.
8 M. Yang, K. Flavin, I. Kopf, G. Radics, C. H. A. Hearnden, G. J. McManus, B. Moran, A. Villalta-Cerdas, L. A. Echegoyen, S. Giordani and E. C. Lavelle, *Small*, 2013, **9**, 4194–4206.
9 S. Giordani, J. Bartelmess, M. Frasconi, I. Biondi, S. Cheung, M. Grossi, D. Wu, L. Echegoyen and D. F. O'Shea, *J. Mater. Chem. B*, 2014, **2**, 7459–7463.
10 J. Bartelmess, E. De Luca, A. Signorelli, M. Baldrighi, M. Becce, R. Brescia, V. Nardone, E. Parisini, L. Echegoyen, P. P. Pompa and S. Giordani, *Nanoscale*, 2014, **6**, 13761–13769.
11 K. Flavin, M. N. Chaur, L. Echegoyen and S. Giordani, *Org. Lett.*, 2010, **12**, 840–843.
12 J. Bartelmess and S. Giordani, *Beilstein J. Nanotechnol.*, 2014, **5**, 1980–1998.
13 M. A. Herranz and N. Martin, in *Carbon Nanotubes and Related Structures: Synthesis, Characterization, Functionalization, and Applications*, ed. D. M. Guldi and N. Martin, Wiley-VCH Verlag GmbH & Co. KGaA, Weinheim, Germany, 2010, pp. 103–134.

14 D. Jain, A. Saha and A. A. Marti, *Chem. Commun.*, 2011, **47**, 2246–2248.
15 F. Li, L. Li, L. Tong, Q. Daniel, M. Goethelid and L. Sun, *Chem. Commun.*, 2014, **50**, 13948–13951.
16 C. Jiang, A. Saha, C. Xiang, C. C. Young, J. M. Tour, M. Pasquali and A. A. Marti, *ACS Nano*, 2013, **7**, 4503–4510.
17 C. Jiang, A. Saha, C. C. Young, D. P. Hashim, C. E. Ramirez, P. M. Ajayan, M. Pasquali and A. A. Marti, *ACS Nano*, 2014, **8**, 9107–9112.
18 G. M. A. Rahman, D. M. Guldi, S. Campidelli and M. Prato, *J. Mater. Chem.*, 2006, **16**, 62–65.
19 E. N. Mhuircheartaigh, S. Giordani and W. J. Blau, *J. Phys. Chem. B*, 2006, **110**, 23136–23141.
20 E. N. Mhuircheartaigh, W. J. Blau, M. Prato and S. Giordani, *Carbon*, 2007, **45**, 2665–2671.
21 J. Bartelmess, A. R. M. Soares, M. V. Martinez-Diaz, M. G. P. M. S. Neves, A. C. Tomé, J. A. S. Cavaleiro, T. Torres and D. M. Guldi, *Chem. Commun.*, 2011, **47**, 3490–3492.
22 M. Ince, J. Bartelmess, D. Kiessling, K. Dirian, M. V. Martinez-Diaz, T. Torres and D. M. Guldi, *Chem. Sci.*, 2012, **3**, 1472–1480.
23 A. Di Crescenzo, I. Kopf, S. Pieraccini, S. Masiero, E. Del Canto, G. P. Spada, S. Giordani and A. Fontana, *Carbon*, 2012, **50**, 4663–4672.
24 Y.-L. Zhao and J. F. Stoddart, *Acc. Chem. Res.*, 2009, **42**, 1161–1171.
25 P. D. Tran, A. Le Goff, J. Heidkamp, B. Jousselme, N. Guillet, S. Palacin, H. Dau, M. Fontecave and V. Artero, *Angew. Chem., Int. Ed.*, 2011, **50**, 1371–1374.
26 F. Li, B. Zhang, X. Li, Y. Jiang, L. Chen, Y. Li and L. Sun, *Angew. Chem.*, 2011, **123**, 12484–12487.
27 B. Reuillard, A. Le Goff and S. Cosnier, *Chem. Commun.*, 2014, **50**, 11731–11734.
28 J. Bartelmess, B. Ballesteros, G. de la Torre, D. Kiessling, S. Campidelli, M. Prato, T. Torres and D. M. Guldi, *J. Am. Chem. Soc.*, 2010, **132**, 16202–16211.
29 C. Ehli, G. M. A. Rahman, N. Jux, D. Balbinot, D. M. Guldi, F. Paolucci, M. Marcaccio, D. Paolucci, M. Melle-Franco, F. Zerbetto, S. Campidelli and M. Prato, *J. Am. Chem. Soc.*, 2006, **128**, 11222–11231.
30 E. Maligaspe, A. S. D. Sandanayaka, T. Hasobe, O. Ito and F. D'Souza, *J. Am. Chem. Soc.*, 2010, **132**, 8158–8164.
31 S. Erbas, A. Gorgulu, M. Kocakusakogullari and E. U. Akkaya, *Chem. Commun.*, 2009, 4956–4958.
32 A. Loudet and K. Burgess, *Chem. Rev.*, 2007, **107**, 4891–4932.
33 G. Ulrich, R. Ziessel and A. Harriman, *Angew. Chem., Int. Ed.*, 2008, **47**, 1184–1201.
34 B. Hinkeldey, A. Schmitt and G. Jung, *ChemPhysChem*, 2008, **9**, 2019–2027.
35 S. Atilgan, T. Ozdemir and E. U. Akkaya, *Org. Lett.*, 2010, **12**, 4792–4795.
36 J. L. Bartels, P. Lu, A. Walker, K. Maurer and K. D. Moeller, *Chem. Commun.*, 2009, 5573–5575.
37 A. Palkar, F. Melin, C. M. Cardona, B. Elliott, A. K. Naskar, D. D. Edie, A. Kumbhar and L. Echegoyen, *Chem.–Asian. J.*, 2007, **2**, 625–633.
38 J. V. Jokerst, A. J. Cole, D. Van de Sompel and S. S. Gambhir, *ACS Nano*, 2012, **6**, 10366–10377.
39 R. Ziessel, C. Goze, G. Ulrich, M. Césario, P. Retailleau, A. Harriman and J. P. Rostron, *Chem.–Eur. J.*, 2005, **11**, 7366–7378.
40 D. Bai, A. Benniston, L. Hagon, H. Lemmetyinen, N. V. Tkachenko, W. Clegg and R. W. Harrington, *Phys. Chem. Chem. Phys.*, 2012, **44**, 4447–4456.
41 J. Bartelmess, M. Baldrighi, V. Nardone, E. Parisini, D. Buck, L. Echegoyen and S. Giordani, *Chem.–Eur. J.*, 2015, DOI: 10.1002/chem.201500877.

